Optoacoustic endoscopy of the gastrointestinal tract

Hailong He[1,2], Ludwig Englert[1,2] and Vasilis Ntziachristos[1,2,*]

[1] Institute of Biological and Medical Imaging, Helmholtz Zentrum München, Neuherberg, Germany

[2] Chair of Biological Imaging at the Central Institute for Translational Cancer Research (TranslaTUM), School of Medicine, Technical University of Munich, Germany

* Corresponding author: Vasilis Ntziachristos, bioimaging.translatum@tum.de

Abbreviations

FOV	Field-of-view
GI	Gastrointestinal
MSOT	Multispectral optoacoustic tomography
OA	Optoacoustic
OCT	Optical coherence tomography
RSOM	Raster-scan optoacoustic mesoscopy
US	Ultrasound

Abstract

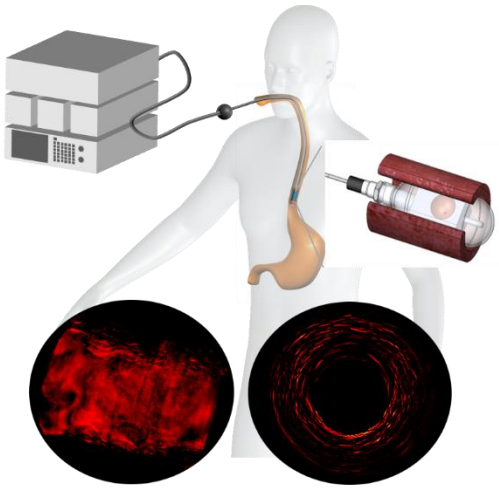

Optical endoscopy is the most commonly applied procedure for inspecting the gastro-intestinal (GI) tract and it is based on different approaches and designs, from using a flexible optical scope to swallowing a small camera capsule that obtains photographs as it advances through the digestive tract. Despite its wide use in GI diagnostics and theranostics, optical visualization only allows a superficial inspection of the wall lining (mucosa), therefore limiting the ability to obtain information from deeper GI layers. In the quest for developing methods to visualize under the mucosal layers, we review herein progress with optoacoustic endoscopy, a technique that captures optical contrast in high resolution deep inside tissues, enabling imaging beneath the surface of the mucosa. Optoacoustic endoscopy combines imaging of optical contrast with the resolution and

depth penetration afforded by ultrasonography, thus merging highly advantageous characteristics for clinical applications. We review progress and the current status of the technology, its key endoscopic competitors, and challenges for clinical application. We further offer a perspective regarding future directions and the overall application potential of the technique to complement the current state-of-the-art.

1. Introduction

Endoscopic imaging plays a vital role in the diagnosis of gastrointestinal (GI) diseases. White light endoscopy (WLE) is the most commonly employed approach today[1]. WLE inserts a flexible optical system (endoscope) into the GI lumen and captures images and video under white light illumination. The result is the visual inspection of the GI wall surface that may show discolorations or abnormal anatomy indicative of disease. Several other techniques have been developed to address the limitations of visual inspection, notably narrow-band imaging (NBI) to enhance WLE contrast, confocal laser endoscopy (CLE) to offer single cell resolution of the mucosa or optical coherence tomography (OCT) to penetrate deeper than WLE[1-4]. While OCT can possibly image deeper than 1 mm in the lumen wall, visualization at several millimetres and beyond is performed with endoscopic ultrasonography (US), which can extend visualization beyond the GI tract wall to adjacent organs, such as the pancreas, or guide biopsies[5].

In the quest to further improve visualization of the GI lumen, endoscopic optoacoustic (photoacoustic) imaging has recently emerged as a technology that enhances contrast and penetration depth, allowing visualization of features never before available to the endoscopic suite. Several review papers have summarized the status and progress of optoacoustic endoscopy for *in vivo* biological studies[6-8]. Optoacoustic imaging resolves optical absorption in tissue with ultrasonic resolution, offering high resolution optical imaging at depths not reached by any other optical method [9, 10], since image formation obeys the laws of ultrasound diffraction, not optical diffusion. A wealth of technological developments over the past decade[10-13], particularly in the field of microscopy and mesoscopy, such as broad bandwidth image formation in the tens to hundreds of MHz range, have enabled in vivo imaging through several millimetres of tissue with resolutions in the 5-50 micrometer range[11]. The technique can resolve different anatomical structures, depending on the wavelength employed, including micro-vasculature, lipids, and mucosal and submucosal anatomy[14]. Illumination at multiple wavelengths further allows imaging of oxygenation and hypoxia using spectral unmixing techniques[11]. These abilities have been employed for dermatological applications, including imaging of cancer or inflammatory disease and treatment[11, 15-19].

This novel ability is also finding its way to the GI tract. The conversion of non-invasive, handheld optoacoustic technology to arrangements that can be inserted into tissue lumen, in an endoscopic fashion, promises to deliver unique optoacoustic imaging performance to the hands of the endoscopist. In this perspective, we review recent advances in OA imaging for clinical applications. We then discuss progress and the technical challenges associated with optoacoustic endoscopy, as well as the current state-of-the-art in imaging performance. Last, we offer an outlook on remaining

requirements toward the mainstream clinical translation of this novel modality to the endoscopy suite.

2. Advances in OA imaging

Optoacoustic imaging illuminates tissue with light of transient energy, typically short photon pulses in the 1-100 nanosecond range. The light energy is absorbed by tissue chromophores, such as hemoglobin, and generates ultrasound waves at the points of absorption, due to thermoplastic expansion [12, 20-22]. The generated ultrasound waves propagate to the surface of the tissue, where they are detected by ultrasound transducers. The signals are collected at multiple positions on the surface and mathematically combined through an inversion process to reconstruct images of optical absorption in tissue, at the wavelength of illumination. Non-invasive clinical optoacoustic imaging is largely achieved by handheld systems that resemble ultrasonography scanners and are typically offered as hybrid optoacoustic-ultrasound implementations. The most common platform today for clinical applications is hand-held Multi-Spectral Optoacoustic Tomography (MSOT), which has already demonstrated a wealth of clinical applications in breast cancer (Fig. 1a) [23, 24], muscular dystrophy [25], Brown Fat activation [26], and the non-invasive visualization of inflammation in the digestive tract associated with Crohn's disease (Fig. 1b)[27]. Other handheld platforms have also been used, primarily for breast cancer imaging (Fig. 1c) [28-31]. The aforementioned hand-held optoacoustic imaging systems operate with frequencies in the MHz range with 100-300 micrometer resolutions at depths of a few centimeters. Besides handheld configurations, a 3D OA tomography system (Fig. 1d) was implemented to image the vasculature of the human breast scanned by arc-shaped ultrasonic transducer arrays with 512 channels, achieving an imaging depth of 4 cm[32]. Compared to the hand-held MSOT system, it can resolve the rich vasculature of the human breast in 3D by using a more complex US recording configuration. However, the 3D OA imaging requires long scanning times of approximately 15 s per wavelength, whereas the hand-held MSOT system can resolve anatomical and spectral features in real-time.

Detectors operating at higher ultrasound frequencies and bandwidths have been employed for higher resolution imaging at more superficial depths, giving rise to mesoscopic imaging applications. Using a transducer array with a 15 MHz central frequency, multispectral OA mesoscopy (MSOM) was developed to image the morphology and function of tumors in vivo in a label-free, non-invasive manner at resolutions of <50 μm throughout the entire tumor mass[33]. Relying on spectral unmixing methods, the patterns of oxygenation, vasculature, and perfusion in breast cancer animal models were resolved across the entire tumor mass, showcasing different levels of structural and functional organization[33]. Operating at even higher frequencies and bandwidths in the range of 10-200 MHz, raster-scan OA mesoscopy (RSOM) achieves resolutions ranging from less than 10 to a few tens of micrometers at penetration depths of several millimeters, depending on the illumination wavelength employed [11, 15-17, 34-36]. RSOM has been applied to a variety of non-invasive applications, such as visualizing microvasculature oxygenation and hypoxia in tissues or tumors, micro-vascular dynamics in response to vascular-targeted therapy[37], distinct vascular patterns in melanomas (Fig. 14)[17], and quantitatively analyzing skin morphology and vascular patterns in psoriasis patients demonstrating the computation of biomarkers associated with inflammatory burden or treatment efficacy[15, 16, 35]. Wavelength selection in a range spanning

the visible and short-wavelength infrared (SWIR) has further enabled the resolution of sebaceous glands, hair, and the distributions of lipids, hemoglobin, melanin, and water in human skin in vivo (Fig. 1f)[14]. Due to the availability of spatial contrast, spectral contrast, and time-dependent imaging, RSOM enables the assessment of anatomical, functional, and molecular features in high-resolution at depths of a few millimeters or even deeper, making it a highly capable tool for GI lumen inspection [11, 38]. Therefore, adaptation of the technology from handheld to endoscopic implementations became the scope of several research investigations as described in the following.

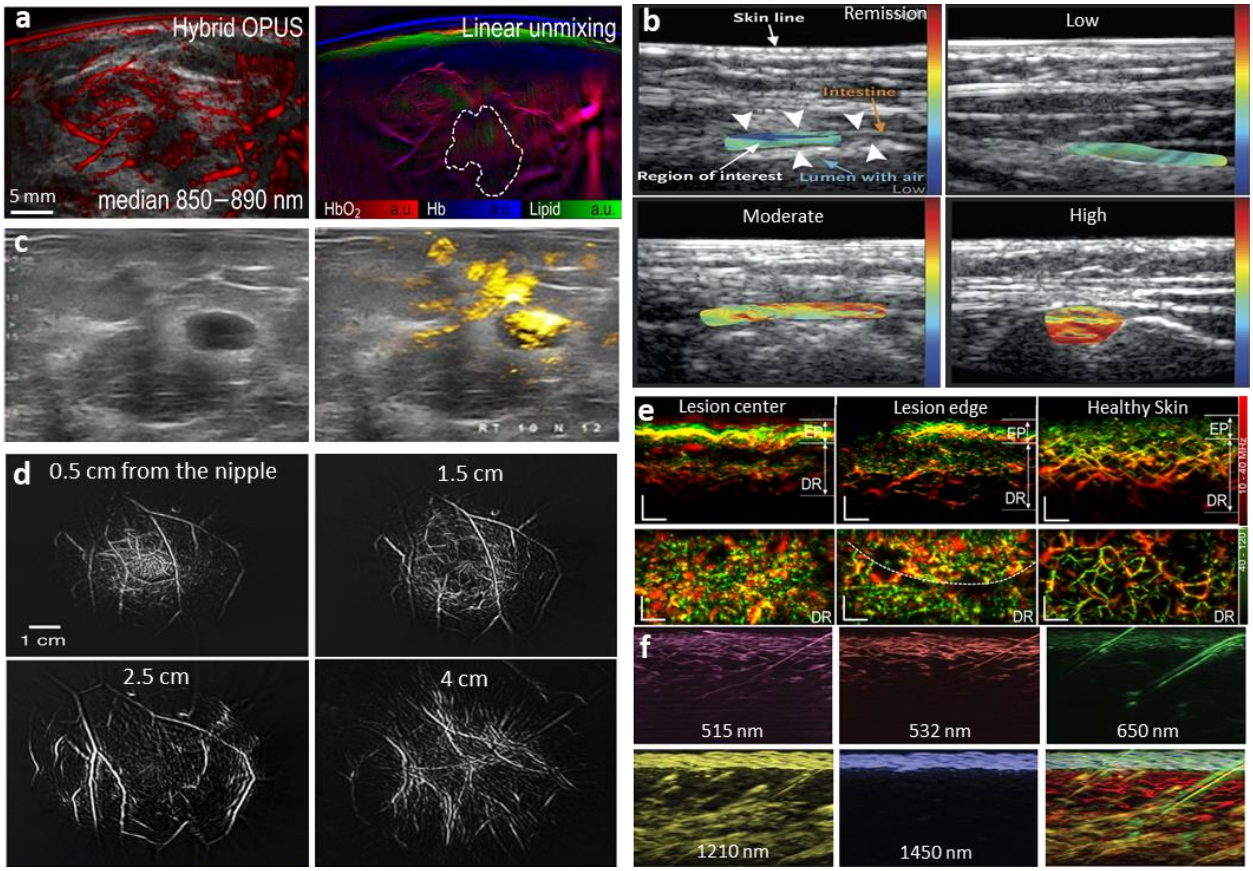

Figure 1. Advances in OA imaging for clinical studies. (a). Hybrid OA/US visualization of breast lesions acquired by a commercial system *Acuity Echo*® (iThera Medical GmbH, Munich, Germany) yields complementary morphologic and functional information by overlaying the OA signals on grayscale US. Linear unmixing affords maps of tissue concentrations of HbO_2, Hb, and lipids. Adapted with permission from Ref. [24]; copyright 2022 Elsevier; distributed under a CC BY 4.0 license. (b). Representative images of MSOT measurements of total hemoglobin in the large bowel and small intestine in patients with different grades of endoscopic disease activity (as evaluated by means of Simplified Endoscopic Score for Crohn's Disease). Adapted with permission from Ref. [27]; copyright 2017 Massachusetts Medical Society. (c). Hybrid OA/US images of breast cancer acquired by a commercial system (Seno Medical Instruments, San Antonio, Texas, USA). The top image depicts morphological image from conventional breast ultrasound of an oval well-circumscribed hypoechoic mass in the right breast and the bottom optoacoustic image shows significantly increased hemoglobin and vasculature within the mass. Adapted with permission from Ref. [29]; copyright 2018 Elsevier; distributed under a CC BY 4.0 license. (d) Vasculature in the right breast of a 27-year-old healthy female volunteer acquired by a 3D OA system. Images at four depths are shown in increasing depth order from the nipple to the chest. Adapted with permission from Ref. [32]. Copyright 2018 Springer Nature. Distributed under a CC BY 4.0 license. (e) RSOM images of a melanoma lesion on a patient's back, revealing the different vascular patterns in the lesion's center, edge, and the surrounding healthy skin. The top row shows cross-sectional RSOM images, while the

second and third rows show the corresponding MIP (maximum intensity projection) images of the epidermis (EP) and dermis (DR) layers in the coronal views. Adapted with permission from ref [17]; copyright 2022 Springer Nature; distributed under a CC BY 4.0 license. (f) Cross-sectional OA images of human skin using RSOM over a wide spectral region, showing the distribution of Hb (microvasculature) and melanin in skin (515 and 532 nm, respectively), melanin in the epidermis and hair (650 nm), subcutaneous fat, sebaceous glands and water content in epidermis (1210 nm), water distribution in the epidermis (1450 nm), and a composite image of all five wavelengths. Adapted with permission from ref [14]. Copyright 2019 Optica Publishing Group.

3. Challenges of OA endoscopy

OA imaging provides rich optical contrast and high resolution at depths that surpass the performance of any optical method, positioning OA endoscopy as an attractive modality for GI diagnostics and theranostics. However, several technical requirements challenge the adaptation of optoacoustic imaging to endoscopic applications:

(1) **US detection.** The thickness of the GI tract in humans varies from a few hundred micrometers to millimeters, while the lumen diameter is in the range of centimeters. In order to fully resolve a segment of the GI lumen wall with high resolution and deep penetration depth, OA endoscopy should combine broad bandwidth for high resolution, high sensitivity for deep tissue imaging, and a small form factor detector so that they can be integrated into a functional scope. Previous work analyzed the necessary broad bandwidth for visualizing esophagus morphology and the selection of components for esophageal optoacoustic endoscopy[39].

(2) **Scanning mode and coupling.** Typical optoacoustic endoscopy designs are based on the single ultrasound transducer that is mechanically rotated and translated within a capsule inserted in the GI lumen in order to offer three dimensional images of the entire wall. This scanning mode can generate large data sets since several centimeter length GI tract segments are scanned with resolutions in the few tens of micrometers or finer, and it is sensitive to motion and the quality of the acoustic coupling of the transducer to the lumen wall.

(3) **Illumination.** Optoacoustic endoscopy demands that tissue illumination is in close proximity to the ultrasound detection element, so that generated signals can be effectively detected, driving the need for a high level of miniaturization and integration so that both illuminating and detection systems can fit into the endoscope. In addition, since the method operates with photon pulses, fast imaging requires light sources with high repetition rates and accurate synchronization with the scanning system[6, 40], while respecting illumination safety limits in terms of the maximum permissible energy (fluence) allowed for tissue imaging.

(4) **Image formation.** Tomographic approaches such as MSOT or RSOM operate by mathematical inversion that utilizes multiple overlapping projections through tissue. In contrast, the image quality and resolution of an endoscopic probe are more dependent on the geometrical characteristics and the resulting sensitivity field and focal length of the ultrasound transducer than on mathematical inversion, due to the outward looking nature of the scan, which limits the availability of overlapping projections through tissue. Therefore, the detector characteristics play a major role in determining image quality and maintain imaging performance over varying diameters of the GI lumen.

Several OA endoscopy implementations have been proposed – incorporating different combinations of solutions to the above challenges – and tested in phantoms, animals, or human tissues, as summarized in (Table I) and reviewed in the following sections.

4. Implementations of optoacoustic endoscopy

Typical designs for OA endoscopy comprise a miniaturized side-collecting US transducer, an illumination waveguide, and a scanning mechanism that can rotate and pull back the optical and ultrasound components for image formation [6, 40-50]. This typical configuration can be divided into scopes that utilize a rotating mechanism that is not inserted into the body (i.e., at the proximal end; Fig.2a), and scopes that utilize a micro-motor that is integrated into the probe that is inserted into the lumen (i.e., at the proximal end; Fig. 2d).

Table 1. Summary of typical OA endoscopy implementations

Study	Probe dimensions	Ultrasound transducers	Resolution	Working distance	Scanning speed	Scanning mechanism	Applications
Kim et al.[40]	1.8 mm (D) 10 mm (L)	40 MHz, PZT, unfocused transducer	17–67 μm (LR) 61–130 μm (AR)	1.46 mm	20 Hz	Torque coil moved by proximal stages	In vivo rat colorectum and mini-swine esophagus
Xie et al.[51]	0.9 mm (D)	40 MHz, PZT, unfocused transducer	250 μm at 2 mm (LR) 100 μm (AR)	1.5 mm	100 Hz	Torque coil moved by proximal stages	In vivo rabbit aorta
Yang et al.[41]	3.8 mm (D) 38 mm (L)	38 MHz, $LiNbO_3$, 2.6 mm (D), 0.5 mm through hole transducer, 5.2 mm (FL)	80 μm (LR) 55 μm (AR)	0.5 mm	4 Hz	Internal micro motor	In vivo rabbit esophagus and rat colon
Ansari et al.[52]	7.4 mm (D) 60 mm (L)	53 MHz, Fabry-Pérot optical sensor, unfocused	60-166 μm (LR) for depths between 1 and 8 mm, 28 μm (AR)	2.5 mm	100 s for a volume*	Proximal end using an x–y scanner	Ex vivo term normal human placenta
He et al.[53]	18.6 mm (D) 20 mm (L)	30 MHz, PVDF, 7 mm (D), 1 mm through hole transducer, 7 mm (FL)	80 μm (LR) 50 μm (AR)	2 mm	2.5 Hz	Torque coil moved by proximal stages	Ex vivo pig esophagus sample
Ali et al.[54]	16 mm (D)	28 MHz, $LiNbO_3$, 6 mm (D), 2 mm through hole transducer, 6 mm (FL)	200 μm (LR) 35 μm (AR)	1.2 mm	50 Hz	External motorized stages	Ex vivo pig esophagus sample

*The volume covers a region 6 mm in diameter. Abbreviations: AR, axial resolution.; D, diameter; FL, focal length; L, length; $LiNbO_3$, planar lithium niobate; TR, transverse resolution; PVDF, polyvinylidene fluoride; PZT: piezoelectric ceramics.

4.1 Scopes with proximal-end rotation

Borrowing designs from optoacoustic intravascular imaging[40, 46, 48, 55], several optoacoustic implementations for endoscopic imaging have used a rotational mechanism at the proximal end of the catheter to synchronously rotate the ultrasound element and an optical waveguide used for illumination by employing a torque coil (**Fig. 2a-c**). The optical wave emits light in proximity to the ultrasound element so that the optoacoustic signals generated can be effectively detected. The optical and acoustic components are typically enclosed in a protective capsule that, depending on its size, can advance either naturally due to peristaltic movement or mechanically by adding a translation stage at the proximal end of the probe, in order to pull back the endoscope and obtain images along the GI tract. The diameter of the scope can be minimized to less than 2 mm for animal applications or operation through the working channel of a WLE scope (**Fig. 2b,c**)[40, 50], or designed for larger diameters (8 mm – 12 mm) for optoacoustic endoscopy in larger animals and

humans[53]. The working distance of optoacoustic endoscopy is determined by the distance between the surface of the endoscopy probe to the objects where optoacoustic signals generate. The minimum working distance of the endoscope depends on the ultrasound transducer characteristics (focal point and focal length) and the overlay geometry formed by the illumination light and the detection view of the detector. This design is challenged by the operational limits of the torque coil with regard to maintaining a consistent rotation speed throughout the examination and achieving the necessary overall rotation speed, due to uncontrolled coil friction producing excessive heat[54]. For example, Furthermore, this design requires a hybrid rotational coupler to pass optical and electrical energy from a stationary system to the rotating endoscope. Such coupling is generally implemented by concentrically aligning a stationary fiber to a rotational fiber and a slip ring to pass electrical (optoacoustic) signals from the rotational unit to a reading system, necessitating precision manufacturing to minimize optical and electrical losses and reduce coupling variations due to rotation.

4.2 Scopes placing the rotating motor at the distal end

An alternative design utilizes a rotating motor at the distal end of the scope, enclosed in a capsule containing optical and acoustic components (**Fig. 2d**). This design approach minimizes friction and improves the smoothness of rotation and overall reliability compared to scopes using a torque coil; however, it reduces the miniaturization potential and requires higher manufacturing precision in order to align the rotating and stationary parts of the probe within the capsule itself. The capsule contains a side-looking ultrasound detector with a central aperture that enable co-axial illumination through the aperture using a miniature optical guide (**Fig.2e**). This coaxial design can enhance the working distance and illumination homogeneity by optimizing the overlay between the illumination and ultrasound detection[41, 42, 44, 53, 54, 56]. The entire optical and ultrasound system is enclosed in a capsule with a 16 mm diameter enabling 360º field-of-view (FOV). Both optical and electrical components are passed through a motor comprising a hollow central shaft. The motor is placed at the proximal end of the capsule and further comprises a slip ring integrated within the capsule and allows the connection of electrical signals. Earlier designs employed a forward looking detector, where the active element is perpendicular to the rotation axis (**Fig. 2f**). In this case, side-view signal detection is enabled by a reflector that re-directs both light and sound by 90 degrees. The micro-motor is placed at the distal end of the capsule and rotates the reflector for rotational scanning. However, forward-looking detectors reduce the angular FOV (250 degrees in Fig. 2f) of the probe because the electrical cables required for micro-motor operation pass through the FOV of the optoacoustic system and block the sound and light over certain angles. Moreover, the use of a reflector increases the length of the capsule (e.g., to 38 mm length and 3.8 mm diameter)[41]. Finally, avoiding the use of the reflector by means of a side looking ultrasound detector design (Fig.2e) eliminates an aberration-prone component from the illumination and detection path, potentially leading to higher image quality.

The specifications of the ultrasound detector determine the image quality and the working distance of the scope. One capsule probe incorporated a side-facing transducer with a planar lithium niobate ($LiNbO_3$) active element and a 28 MHz-central frequency, as well as a 6 mm focal length and a 2

mm central aperture to allow coaxial illumination (Fig. 2e). The axial and transverse resolutions were measured as 35 and 200 µm, respectively. The side-view detector's focal plane was 2 mm from the capsule surface yielding a 700 µm depth of focus, which allowed imaging of a large lumen with a 360º FOV. In another example, a miniaturized optoacoustic endoscopy probe featured a focused ultrasound detector (1.8 mm diameter, 4 mm focal length, Fig. 2f) [44]. In this case, the optoacoustic waves pass through the reflector, which requires a longer focal distance and yielding a focal plane ~ 800 µm from the endoscope's surface. This short working distance limits the probe to imaging the GI tracts of small animals (a few millimeters in diameter).

Fig. 2g illustrates the working principle of a potential clinical optoacoustic capsule endoscopy system. In such a system, the capsule-shaped probe would be comparable in size to a human or pig esophageal lumen and host the US transducer and illumination scheme. A guiding wire or a tether could advance and control the capsule, with the tether being more applicable to esophageal imaging. For human measurements, the capsule probe would be swallowed and gradually moved through the upper GI tract under the natural propulsion force of peristalsis. Once the probe reaches the distal-most region of interest, the esophageal wall would constrict around the capsule, stabilizing and centering the capsule inside the lumen, which should stabilize the endoscopy probe inside the capsule and reduce motion artifacts during in vivo volumetric scanning. OA waves and laser light could pass through the detection window of the capsule, while volumetric images with the same length of the detection window could be obtained without moving the capsule. The capsule could then be repositioned to image other regions of the esophageal wall. The capsule design could potentially afford higher image quality compared to miniaturized probes designed to operate through the working channel of WLE, but lacks the anatomical reference provided by WLE and other optical endoscopic approaches, a limitation that could be addressed by adding a camera at the front end of the capsule. Perhaps the more critical limitation is the absence of a working channel to allow biopsies and other procedures. In that respect, an optoacoustic endoscope based on a capsule design would be more suited to screening for suspicious tissue or lesions to be investigated in a follow up procedure with a conventional endoscope comprising a working channel. To enable such application, it is critical to develop co-localization approaches of the two scopes based on imaging features and mechanical measurements of the distance using the tethered line or other means.

A prototype of such a capsule optoacoustic endoscopy system was built and tested on excised pig esophageal tissue (Fig. 2h) [54]. For optoacoustic signal generation, the system employed a rapid laser source with a 532 nm wavelength and a repetition rate in the rage of 1-100 kHz, which enabled B-scan frame rates as high as 50 Hz. The illumination was coupled to a multimode optical fiber with a core diameter of 105 µm and a numerical aperture of 0.2. A 90-degree silver coated optical reflector facilitated side illumination. A 360-degree unobstructed FOV was enabled by employing a customized low-friction miniature gold slip ring for electrical coupling of high frequency ultrasound signal transmission, avoiding obstruction from driving cables over the FOV. During rotational scanning, the recorded optoacoustic signals were pre-amplified externally with a 30 dB amplifier prior to data acquisition. For this prototype system, the capsule was controlled by an external linear motorized stage that, in combination with the in-capsule motor, enabled helical pull-back scans [2].

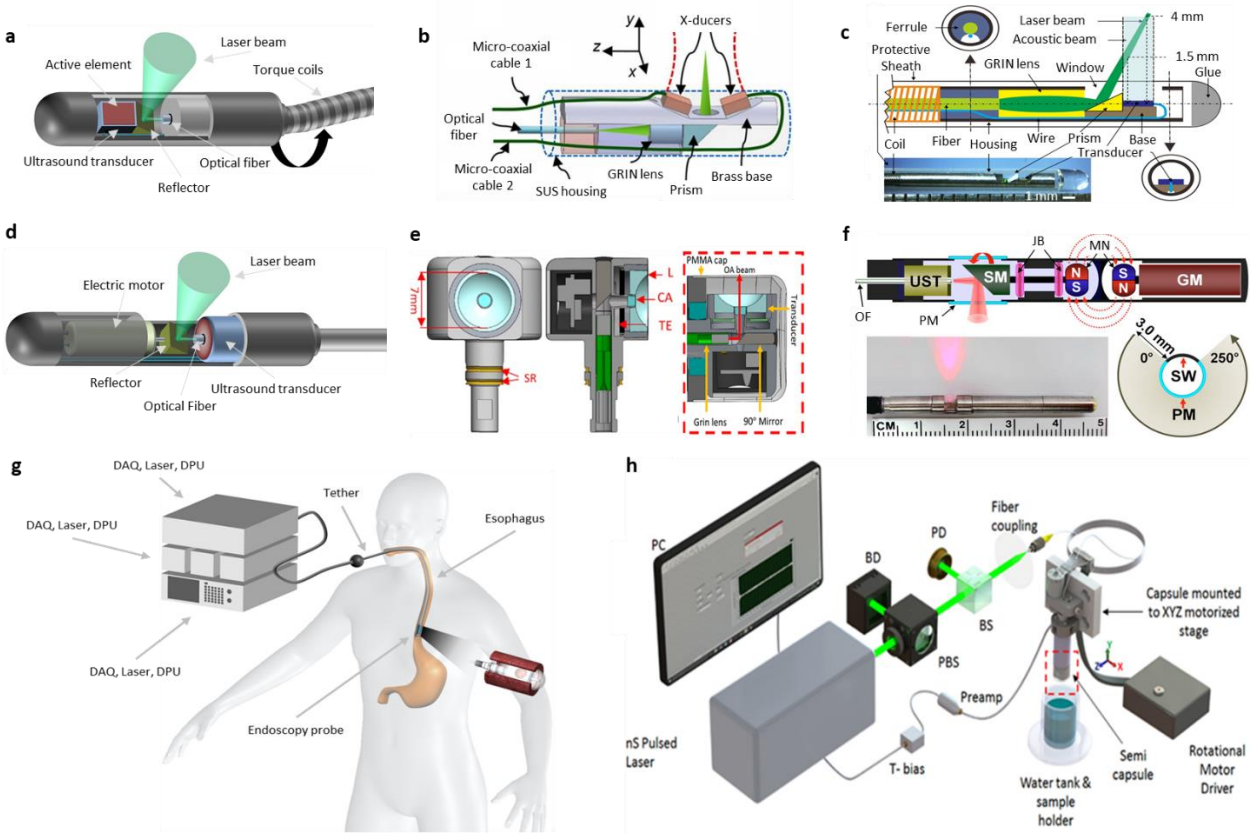

Figure 2. Representative implementations of OA endoscopy systems. (a) Schematic principle of an externally (proximally) rotated endoscopic probe. (b) Schematic of a proximally rotated OA endoscope with a side-facing transducer adjacent to the illumination beam. Reprinted with permission from ref [40]; copyright 2022 Elsevier; distributed under a CC BY-NC-ND license. (c) Schematic and photograph of the proximal end rotation design with a single transducer above the reflector. Reprinted with permission from ref [50]; Copyright 2018 Wiley-VCH. (d) Schematic principle of an endoscopic probe with a rotating motor at the distal end. (e) Schematic cross-sectional and en-face view of an endoscope transducer with a central aperture and the benchtop optoacoustic endoscopy experimental setup; TE: Transducer element, EC: Electrical Connector, L: Acoustic Lens, CA: Central Aperture Window, SR: Slip rings. Adapted with permission from ref [54]; copyright 2019 Elsevier; distributed under a CC BY 4.0 license. (f) Photograph and schematic principle of a probe with a motorized reflector. GM, geared micromotor; GP, glass partition; JB, jewel bearings; MN, magnets; OF, optical fiber; PM, plastic membrane (imaging window); SM, scanning mirror; SW, signal wire; UST, ultrasonic transducer; WM, water medium. Reprinted with permission from ref [44]; copyright 2012 Optica Publishing Group. (g) Schematic principle of a potential OA endoscopy system designed for the human esophagus. (h) Benchtop optoacoustic capsule endoscopy experimental setup. PBS: polarizing beam splitter, BS: beam splitter, BD: beam dump, PD: photodiode. Adapted with permission from ref [54]; copyright 2019 Elsevier; distributed under a CC BY 4.0 license.

4.3 Optoacoustic endoscopy based on optical ultrasound sensors

Aside from motorized designs, flexible OA scopes were also introduced for forward-viewing tissue imaging [52, 57]. In one implementation, a 7.4 mm diameter scope (Fig. 3a) was constructed using a planar Fabry–Pérot sensor for detection, which is an optical resonator comprising a thin film of polymer between two mirrors or reflecting surfaces that are interrogated with a focused laser beam from a continuous wave tunable laser[58]. This endoscope was built from a coherent multicore fiber bundle with a Fabry–Pérot resonator at its distal end. Scanning over each fiber core at its proximal

end using an x-y scanner mimics a dense array of ultrasound transducers for tomography imaging. The optoacoustic excitation illumination is delivered through the Fabry–Pérot sensor through an array of multimode fibers distributed circumferentially around the sensor's fiber bundle. The planar Fabry-Perot US sensor enables measurements over a high density grid in the forward sense. However, one image requires approximately 100 s to collect due to the low repetition rate of the excitation laser source, which is slow for human applications and indicates the need for further technological improvements to the design. In addition, a recent work (Fig. 3b) reported a miniaturized optoacoustic endoscope that comprises multimode fibers for illumination and an optical sensor based on a single mode fiber with plano-concave microresonator for ultrasound detection[59].

One of the key advantages of this forward-viewing probe is that the scope could be integrated in the working channel of a white light endoscope and used to augment conventional endoscopic procedures. Conversely, forward-viewing systems are limited by their small fields-of-view and need for precision targeting to obtain an image from the desired location. Therefore, forward-viewing endoscopes are more suited for "optical biopsies" (precision optical measurements in place of a tissue biopsy) that for GI tract inspection.

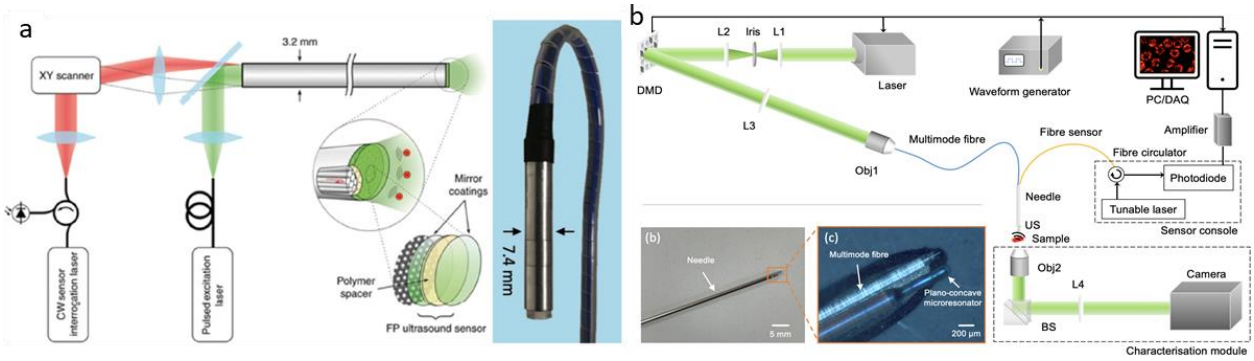

Figure 3. Optoacoustic endoscopy based on optical sensor**.** a. Schematic representation of an OA Fabry-Pérot-based endoscopy probe with magnified visualization of the distal end showing the individual fiber-optic cores in the coherent fiber bundle and the Fabry-Pérot US sensor. The sensor is comprised of two dielectric mirror coatings separated by a polymer (Parylene C) spacer layer. Photograph of the probe (right side). Adapted with permission from ref [52, 57]; copyright 2020 Optica Publishing Group; copyright 2018 Springer Nature; both distributed under a CC BY 4.0 license. b. Illustration of an optoacoustic endoscopy with optical resolution. The imaging probe is integrated within a spinal needle (20 gauge). The needle has an outer diameter of 0.9 mm and an inner diameter of 0.6 mm. L1-4, achromatic doublet lenses; DMD: digital micromirror device; US, ultrasound; Obj1-2: Objective lenses; BS: beamsplitters; PC: personal computer; DAQ: data acquisition. Adapted with permission from ref [59], copyright 2022 Optica Publishing Group.

5. Optoacoustic endoscopy applications

Based on the aforementioned designs, the capabilities of various optoacoustic endoscopy probes have been tested on excised tissue or in vivo animals. A proximally rotated optoacoustic endoscope using interchangeable side-looking 15 MHz and 50 MHz intravascular US (IVUS) detectors was employed to image excised pig esophageal tissue (Fig. 4a)[60]. For these ex vivo experiments, 6 cm esophageal sections were inserted into polyethylene tubes, immersed in water for acoustic coupling, and imaged along several sections using linear or radial scanning using both transducers. The

results of the study suggested that a broader ultrasound bandwidth, extending from 10-100 MHz, was necessary to reveal critical tissue features, such as microvasculature, during esophageal imaging[60], an observation that corroborated the findings of non-endoscopic RSOM.

In vivo optoacoustic endoscopy of a rat colon was performed with a proximal-rotation scope design (Fig. 4b), affording images of superficial vasculature and other morphological features at resolutions up to 13 µm in the transverse direction and 61 µm in the radial direction. However, these resolutions were obtained by focusing the illumination light with a GRIN lens, resulting in very limited penetration depth[40]. Simultaneous OA and US structural imaging of the esophagus, colon, and neighbouring tissues in the GI tracts of rabbits and rats in vivo was performed with a 2.8 mm × 38 mm endoscope based on a reflector and driven by a distal micro-motors (Fig. 4c) [41, 42, 44]. Dual wavelength measurements (562 nm and 584 nm) visualized the oxygen saturation (SO_2) of a rat colon, albeit at a reduced FOV of 270° due to the obstruction caused by the electrical wiring of the micro-motor[41]. The most recent endoscope implementation was reduced in size to 2.5 mm to fit through the working channel of a standard video endoscope, while the angular FOV during rat colon imaging was increased to 310° (Fig. 4d)[44].

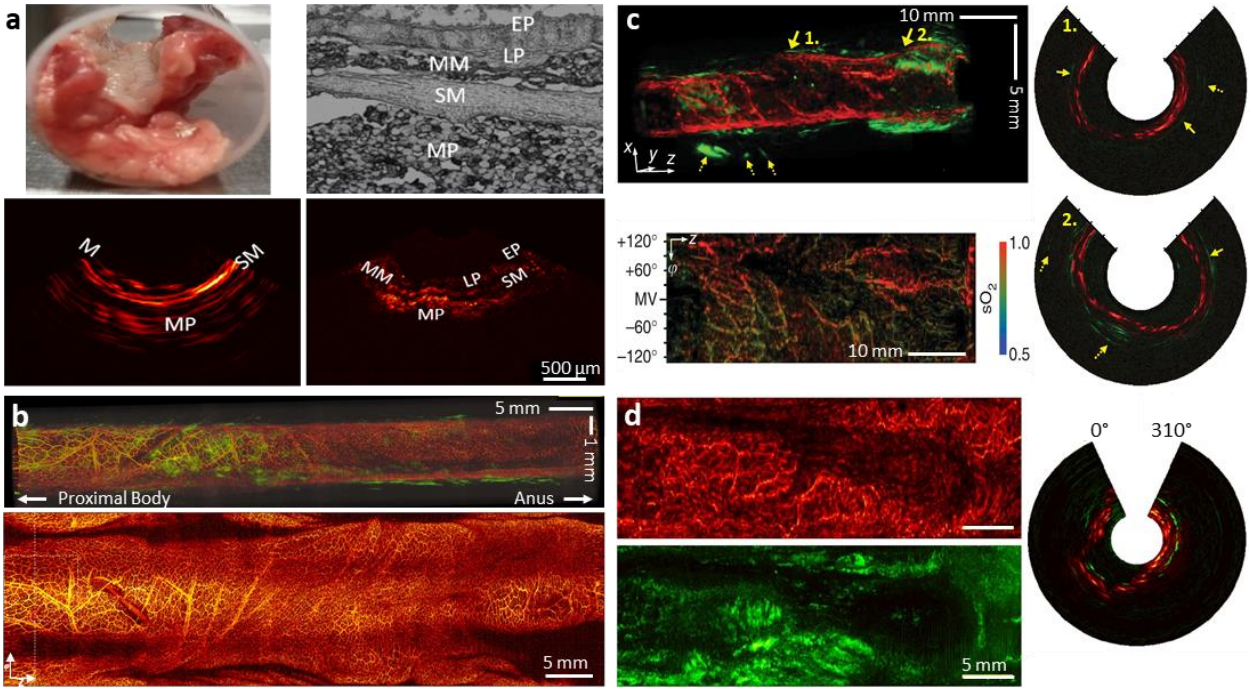

Figure 4. Preclinical testing of OA endoscopy systems. (a) Imaging of an ex vivo pig esophagus using 15 and 50 MHz transducers. Photograph of esophageal tissue in a cylindrical sample holder (upper left), an unstained histological image of a longitudinal section of the sample (upper right), and OA images generated using data from 15 MHz (lower left) and 50 MHz (lower right) detectors. Adapted with permission from ref [60]; copyright 2018 IEEE. (b) 3D-rendered OA (red) and US (green) endoscopic images of a rat colon in vivo. MIP OA endoscopy image (below in red). Adapted with permission from ref [40]; copyright 2022 Elsevier. (c) Overlayed endoscopic OA (red) and US (green) images of a rat colon (upper left panel). Cross-sectional images with a 270° FOV from the position indicated by arrows 1 and 2 in the upper left panel (right panel). Ultrasonic radial maximum amplitude projection (MAP) image showing the echogenicity distribution (lower left panel). Adapted with permission from ref [41]; copyright 2012 Springer Nature. (d) Endoscopic OA (red) and US (green) structural MAP images of an in vivo rat colon (left panel) and a 310° cross-sectional image (right panel). Adapted with permission from ref [44]; copyright 2012 Optica Publishing Group.

While the abovementioned studies provide proof-of-principle for the potential of OA endoscopy in small animals (Fig.4), recent developments are geared toward systems that would be appropriate for human applications [53, 54]. Due to the larger size afforded by the human GI tract, stand-alone scopes based on capsules (Fig. 2e) could employ higher sensitivity ultrasound transducers and better geometrical characteristics than scopes designed for animals or for operation through the working channel of WLE scopes. These larger capsules and transducers could enable favorable designs of the ultrasound sensitivity field, leading to higher image quality compared with smaller detector elements. Complete 360 degree viewing angles were recently demonstrated in an OA capsule probe employing micromotors to concentrically drive the optical and electrical circuitry (Fig. 2d)[53, 54], solving the limited view of older designs based on rotating reflectors (Fig. 2f)[44, 61]. Moreover, the larger capsule dimensions allowed by the human GI-tract, potentially optimizes acoustic coupling by capitalizing on the peristaltic movement of the GI tract that can engulf the capsule and maximize contact to the lumen wall, in analogy to tethered capsule designs developed for endoscopic Optical Coherence Tomography [2].

Optoacoustic endoscopy with a large (human-appropriate) capsule was demonstrated in a pig esophagus ex vivo (Fig. 5a). The system used for the study[53] employed a high-sensitive ultrasound detector with a 7 mm focal length and enabled for the first time 360-degree images of the entire segment with a transverse resolution of 80 μm and a radial resolution of 55 μm. The vascular structure of the esophageal wall was resolved within the mucosal and submucosal layers as confirmed by histological staining with hematoxylin and eosin and immunohistochemistry for vascular marker CD31 (Fig. 5a). This comparison with histology also showed that the vascular morphology of the esophageal wall can be resolved as deep as 2 mm below the surface. Using a higher sensitivity transducer and faster laser source, full 360 degree FOV imaging of a swine esophagus sample mounted inside a 50 mL falcon tube (Fig. 5b) was also demonstrated[54]. A 3D volume of the esophagus sample was imaged by a pullback scan at 50 Hz B-scan rate over a distance of 12 mm at 2.4 mm/s. The full scan was completed in 5 seconds with an arc sampling resolution of 31.4 μm at focus, an axial sampling resolution of 3 μm, and a helical pitch of 48 μm. This improved implementation achieved a 20-fold increase in the B-scan frame rate compared to the proximal rotation design by integrating the rotation coupling directly onto the transducer housing inside the capsule with customized miniature slip rings [53]. In the 2D enface and axial MIPs generated from the helical scan, the fiducial marker and capsule surface were highlighted. In addition, blood vessels of the esophagus tissue were visualized over the 360-degree FOV at a penetration depth up to 1.2 mm. Beside capsule optoacoustic endoscopy, the Fabry-Pérot sensor based endoscopy has applied to measure ex vivo human placenta (Fig. 5c) [52]. A water-based gel was used for acoustic coupling and optoacoustic signals were excited at the wavelength of 750 nm. The superficial vasculature of the chorionic surface of the human placenta sample was visualized by wide-field microscopy while the corresponding OA images visualizes the depth-resolved vasculature through 2.5 mm of tissue.

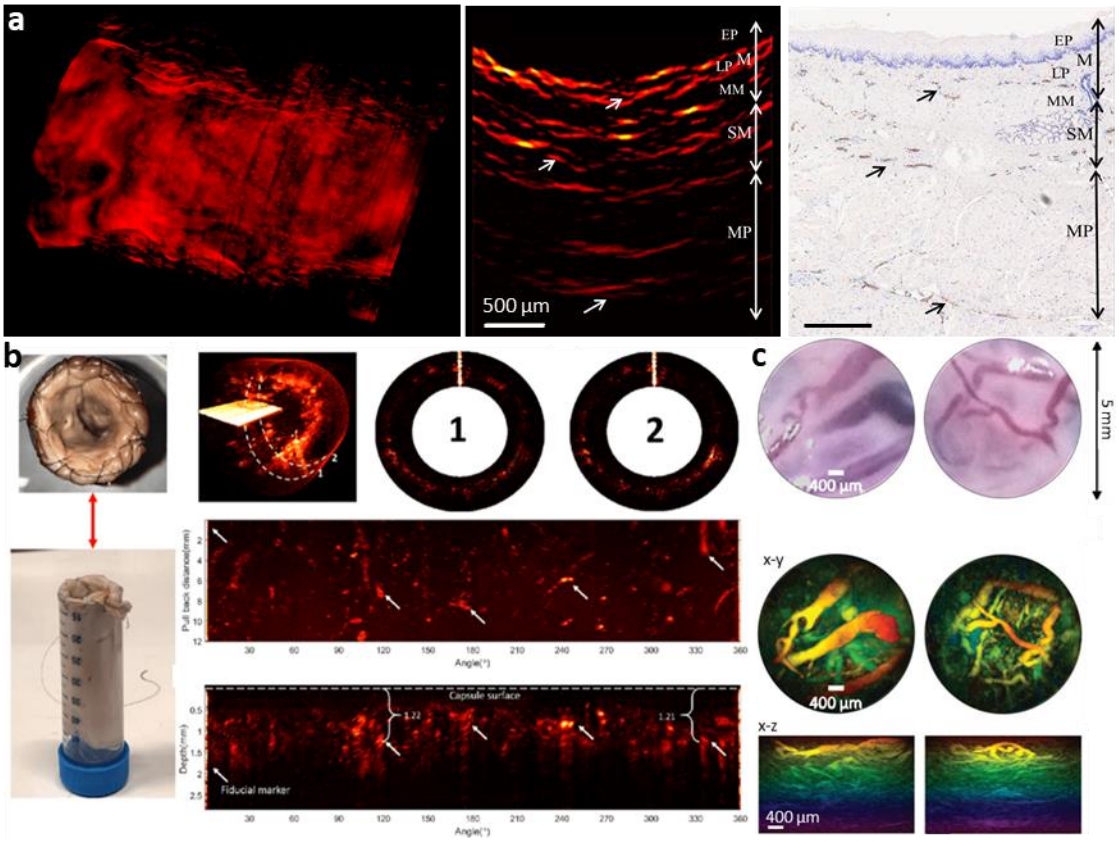

Figure 5. OA imaging of excised pig esophagus and human tissue. (a) Volumetric image of a pig esophagus sample imaged with tethered-capsule OA endoscopy (upper panel) and an enlarged image (indicated by dash lines) with the vasculature (marked by white and black arrows) of the different esophageal layers revealed by anti-CD31 immunostaining (lower right panel). EP, epithelium (sublayer of the mucosa); LP, lamina propria (sublayer of the mucosa); M, mucosa; MM, muscularis mucosa (sublayer of the mucosa); MP, muscularis propria; SM, submucosa. Adapted with permission from ref [53]; copyright 2019 Wiley-VCH; distributed under a CC BY 4.0 license. (b) 360° helical volumetric scan of an ex vivo female pig esophagus over a 12 mm longitudinal pullback. The sample was mounted on a 50 mL Falcon tube for support. The 3D volumetric render of the helical scan and the corresponding 2D enface and axial maximum intensity projections were shown. Adapted with permission from ref [54]; copyright 2019 Elsevier; distributed under a CC BY 4.0 license. (c) Widefield microscope images of an ex vivo term normal human placenta (upper panel), and Fabry-Pérot based endoscopic OA maximum intensity projection images from the same area showing depth-resolved vascular structures (middle and bottom panel). Adapted with permission from ref [52, 57]; copyright 2020 Optica Publishing Group; copyright 2018 Springer Nature; both distributed under a CC BY 4.0 license.

6. Outlook

OA imaging has demonstrated unique abilities to visualize optical contrast in high-resolution in tissues, reaching deeper than optical microscopy methods. OA endoscopy images tissue vasculature without the need for contrast agents at various depths, depending on the wavelength employed. Moreover, endoscopic imaging can be applied with illumination in two or more wavelengths to resolve oxygenated and deoxygenated hemoglobin and compute tissue oxygenation and hypoxia[11]. Such measurements could offer additional information on disease development and infiltration, being able to also identify tissue alterations under the GI-wall surface throughout the tissue segment imaged. Therefore they offer the potential to characterize functional

features of disease that are not generally visualized today[62]. Of particular further interest are metabolic readings that can be offered with optoacoustic technology using label free measurements[63]. While these abilities have not yet been demonstrated in vivo, the possibility is there to adapt multi-wavelength imaging to potentially also offer such functional measurements.

In terms of imaging performance, the properties of the ultrasound detector used are critical in optoacoustic endoscopy systems. For the human GI lumen wall, the thickness of the mucosa and submucosa in the human esophageal wall varies from a few hundred micrometers to millimeters, whereby the size of blood capillaries and vessels in different layers of the esophageal wall range from several micrometers, typically located in the superficial lamina propria, to larger vessels with a diameter of up to a hundred micrometers in deeper layers[64]. Thus, the frequency content of OA signals generated in the esophageal wall is intrinsically broadband because it depends of the size of the absorber that generates the ultrasound signal detected. Previous work has demonstrated that ultra-wide bandwidth transducers ranging from a few to 100 MHz are necessary for high quality OA imaging, and can impart the ability to resolve the layers of the esophageal wall[60]. Further studies are required to find a reasonable balance between resolution and imaging depth in order to permit high quality imaging in the human GI tract for disease diagnosis. Moreover, the image resolution and penetration depth achieved in OA endoscopy depends on the focusing width and depth of focus of the US transducers. This is because, in contrast to conventional optoacoustic mesocopy [11], optoacoustic signal collection during endoscopic measurements does not afford highly overlapping projections due to the collection geometry of the outward-looking detector. Typical spherical focused transducers in OA imaging achieve transverse resolutions in the range of tens of micrometers, but their depth-of-focus is limited to a few hundreds of micrometers by nature of their spherical geometry, restricting the penetration depth in OA endoscopy. In contrast, transducers with axicon geometry could be a better option as they yield pencil-shaped beam sensitivity profiles with high transverse resolution over an extended depth of focus. One study utilized a conical transducer that produced a pencil beam OA detection profile 81 MHz (−3 dB) broadband and a exceeding 1 mm depth of focus, with a retained 40 μm transverse resolution over a 950 μm axial distance[65], which could allow for high resolution and a much deeper penetration depth of GI tissue compared to spherical focused transducers.

In comparison to conventional piezoelectric US transducers, optical-based sensors have been reported to provide advantageous features including wide bandwidth, high sensitivity, miniature size, and immunity to electromagnetic interference[57, 66-68], and they provide an interesting alternative for endoscopic implementations. In addition, because of their transparency, optical-based sensors could be integrated with the illumination components, which could then lead to co-axial designs of OA endoscopy for excitation and detection signals, allowing for the miniaturization of the probe and improvement of the detection performance.

The illumination specifications are also critical to the performance of OA endoscopes. The superficial vasculature of the GI tract can be visualized well using a single wavelength (e.g., 532 nm) from Q-switched solid-state lasers that offer a high repetition rate (in the range of up to tens of kHz) and sufficient laser pulse energy. However, visualization deeper in tissue, as it relates to GI lesions occurring in the submucosa, may be better achieved via red-shifted lasers. In the red

part of the spectrum, one can reach a balance of a depth and contrast by carefully selecting the illuminating wavelength. Q-switch pumped OPO (optical parametric oscillator) systems have been used to implement a multispectral OA imaging system[10, 12]. However, in addition to being bulky in size and high-cost, the low pulse repetition rate and wavelength-tuning speed of OPO systems significantly limit the imaging speed, making them impractical for in vivo 3D endoscopy imaging. For this reason laser diodes (LD) and light emitting diodes (LED) have demonstrated potential as promising alternatives to solid-state laser sources for OA imaging[69-72]. These new laser sources can provide high repetition rates and a wide range of wavelengths and are also low-cost. These advantages could allow for real-time OA endoscopic imaging of the human GI lumen wall with similar scanning speeds to OCT endoscopy, an imaging modality that has already been validated for the clinical environment. LD or LED light sources, however, currently provide low output energies, which could lead to low signal quality. Therefore, highly powerful LD or LED sources must be developed, further integrated as an array, and combined with a high-sensitivity US detection scheme for optimal OA endoscopy.

Overall, OA endoscopy has shown promise for clinical application in the last decade, with designs approaching the requirements for in vivo human measurements. The method has demonstrated high resolution 360-degree scans of long tissue segments in vivo and ex vivo, presenting the possibility to enhance optical endoscopy with sub-surface visualization and new contrast mechanisms, even when no contrast agents are employed. With continuous technical breakthroughs such as novel detector designs, enhances in sensitivity and novel light sources, OA endoscopy has great translational potential in supporting current clinical endoscopic applications to improve GI disease detection and management.

Funding

This project has received funding from the European Union's Horizon 2020 research and innovation program under ESOTRAC (Grant no. 732720 to V.N.) and WINTHER (Grant no. 871763 to V.N.). We thank Dr. Robert J. Wilson and Dr. Gabriella Leung for their attentive reading and improvements of the manuscript

Conflict of Interest

V.N. is a founder and equity owner of sThesis GmbH, iThera Medical GmbH, Spear UG, and i3 Inc.

References

1. Mannath, J.; Ragunath, K., Role of endoscopy in early oesophageal cancer. *Nature reviews. Gastroenterology & hepatology* **2016**.
2. Gora, M. J.; Sauk, J. S.; Carruth, R. W.; Gallagher, K. A.; Suter, M. J.; Nishioka, N. S.; Kava, L. E.; Rosenberg, M.; Bouma, B. E.; Tearney, G. J., Tethered capsule endomicroscopy enables less invasive imaging of gastrointestinal tract microstructure. *Nature medicine* **2013,** *19* (2), 238-40.
3. Vakoc, B. J.; Fukumura, D.; Jain, R. K.; Bouma, B. E., Cancer imaging by optical coherence tomography: preclinical progress and clinical potential. *Nature reviews. Cancer* **2012,** *12* (5), 363-8.

4. Goetz, M.; Malek, N. P.; Kiesslich, R., Microscopic imaging in endoscopy: endomicroscopy and endocytoscopy. *Nature reviews. Gastroenterology & hepatology* **2014,** *11* (1), 11-8.
5. Kirtane, T. S.; Wagh, M. S., Endoscopic Optical Coherence Tomography (OCT): Advances in Gastrointestinal Imaging. *Gastroenterology research and practice* **2014,** *2014*, 376367.
6. Guo, H.; Li, Y.; Qi, W.; Xi, L., Photoacoustic endoscopy: A progress review. *J Biophotonics* **2020,** *13* (12), e202000217.
7. Li, Y.; Lu, G.; Zhou, Q.; Chen, Z., Advances in Endoscopic Photoacoustic Imaging. *Photonics* **2021,** *8* (7).
8. Yoon, T. J.; Cho, Y. S., Recent advances in photoacoustic endoscopy. *World journal of gastrointestinal endoscopy* **2013,** *5* (11), 534-9.
9. Ntziachristos, V., Going deeper than microscopy: the optical imaging frontier in biology. *Nat Methods* **2010,** *7* (8), 603-14.
10. Taruttis, A.; Ntziachristos, V., Advances in real-time multispectral optoacoustic imaging and its applications. *Nat Photonics* **2015,** *9* (4), 219-227.
11. Omar, M.; Aguirre, J.; Ntziachristos, V., Optoacoustic mesoscopy for biomedicine. *Nat Biomed Eng* **2019,** *3* (5), 354-370.
12. Razansky, D.; Distel, M.; Vinegoni, C.; Ma, R.; Perrimon, N.; Koster, R. W.; Ntziachristos, V., Multispectral opto-acoustic tomography of deep-seated fluorescent proteins in vivo. *Nat Photonics* **2009,** *3* (7), 412-417.
13. Lin, L.; Hu, P.; Tong, X.; Na, S.; Cao, R.; Yuan, X.; Garrett, D. C.; Shi, J.; Maslov, K.; Wang, L. V., High-speed three-dimensional photoacoustic computed tomography for preclinical research and clinical translation. *Nat Commun* **2021,** *12* (1), 882.
14. Berezhnoi, A.; Aguirre, J.; Hindelang, B.; Garzorz-Stark, N.; Omar, M.; Darsow, U.; Eyerich, K.; Ntziachristos, V., Optical features of human skin revealed by optoacoustic mesoscopy in the visible and short-wave infrared regions. *Opt Lett* **2019,** *44* (17), 4119-4122.
15. Aguirre, J.; Schwarz, M.; Garzorz, N.; Omar, M.; Buehler, A.; Eyerich, K.; Ntziachristos, V., Precision assessment of label-free psoriasis biomarkers with ultra-broadband optoacoustic mesoscopy. *Nat Biomed Eng* **2017,** *1* (5), 0068.
16. Hindelang, B.; Nau, T.; Englert, L.; Berezhnoi, A.; Lauffer, F.; Darsow, U.; Biedermann, T.; Eyerich, K.; Aguirre, J.; Ntziachristos, V., Enabling precision monitoring of psoriasis treatment by optoacoustic mesoscopy. *Sci Transl Med* **2022,** *14* (644), eabm8059.
17. He, H.; Schonmann, C.; Schwarz, M.; Hindelang, B.; Berezhnoi, A.; Steimle-Grauer, S. A.; Darsow, U.; Aguirre, J.; Ntziachristos, V., Fast raster-scan optoacoustic mesoscopy enables assessment of human melanoma microvasculature in vivo. *Nat Commun* **2022,** *13* (1), 2803.
18. Wang, Y.; Xu, D.; Yang, S.; Xing, D., Toward in vivo biopsy of melanoma based on photoacoustic and ultrasound dual imaging with an integrated detector. *Biomed Opt Express* **2016,** *7* (2), 279-86.
19. Hindelang, B.; Aguirre, J.; Berezhnoi, A.; He, H.; Eyerich, K.; Ntziachristos, V.; Biedermann, T.; Darsow, U., Optoacoustic mesoscopy shows potential to increase accuracy of allergy patch testing. *Contact Dermatitis* **2020,** *83* (3), 206-214.
20. Kruger, R. A.; Liu, P.; Fang, Y. R.; Appledorn, C. R., Photoacoustic ultrasound (PAUS)--reconstruction tomography. *Med Phys* **1995,** *22* (10), 1605-9.
21. Xu, M. H.; Wang, L. H. V., Photoacoustic imaging in biomedicine. *Rev Sci Instrum* **2006,** *77* (4), 041101.
22. Wu, L. W. a. H.-I., Biomedical Optics principles and imaging. *Wiley-Interscience* **2007**.
23. Diot, G.; Metz, S.; Noske, A.; Liapis, E.; Schroeder, B.; Ovsepian, S. V.; Meier, R.; Rummeny, E.; Ntziachristos, V., Multispectral Optoacoustic Tomography (MSOT) of Human Breast Cancer. *Clin Cancer Res* **2017,** *23* (22), 6912-6922.

24. Kukacka, J.; Metz, S.; Dehner, C.; Muckenhuber, A.; Paul-Yuan, K.; Karlas, A.; Fallenberg, E. M.; Rummeny, E.; Justel, D.; Ntziachristos, V., Image processing improvements afford second-generation handheld optoacoustic imaging of breast cancer patients. *Photoacoustics* **2022,** *26*, 100343.
25. Regensburger, A. P.; Fonteyne, L. M.; Jungert, J.; Wagner, A. L.; Gerhalter, T.; Nagel, A. M.; Heiss, R.; Flenkenthaler, F.; Qurashi, M.; Neurath, M. F.; Klymiuk, N.; Kemter, E.; Frohlich, T.; Uder, M.; Woelfle, J.; Rascher, W.; Trollmann, R.; Wolf, E.; Waldner, M. J.; Knieling, F., Detection of collagens by multispectral optoacoustic tomography as an imaging biomarker for Duchenne muscular dystrophy. *Nat Med* **2019,** *25* (12), 1905-1915.
26. Reber, J.; Willershauser, M.; Karlas, A.; Paul-Yuan, K.; Diot, G.; Franz, D.; Fromme, T.; Ovsepian, S. V.; Beziere, N.; Dubikovskaya, E.; Karampinos, D. C.; Holzapfel, C.; Hauner, H.; Klingenspor, M.; Ntziachristos, V., Non-invasive Measurement of Brown Fat Metabolism Based on Optoacoustic Imaging of Hemoglobin Gradients. *Cell Metab* **2018,** *27* (3), 689-701 e4.
27. Knieling, F.; Neufert, C.; Hartmann, A.; Claussen, J.; Urich, A.; Egger, C.; Vetter, M.; Fischer, S.; Pfeifer, L.; Hagel, A.; Kielisch, C.; Gortz, R. S.; Wildner, D.; Engel, M.; Rother, J.; Uter, W.; Siebler, J.; Atreya, R.; Rascher, W.; Strobel, D.; Neurath, M. F.; Waldner, M. J., Multispectral Optoacoustic Tomography for Assessment of Crohn's Disease Activity. *N Engl J Med* **2017,** *376* (13), 1292-1294.
28. Dogan, B. E.; Menezes, G. L. G.; Butler, R. S.; Neuschler, E. I.; Aitchison, R.; Lavin, P. T.; Tucker, F. L.; Grobmyer, S. R.; Otto, P. M.; Stavros, A. T., Optoacoustic Imaging and Gray-Scale US Features of Breast Cancers: Correlation with Molecular Subtypes. *Radiology* **2019,** *292* (3), 564-572.
29. Oraevsky, A. A.; Clingman, B.; Zalev, J.; Stavros, A. T.; Yang, W. T.; Parikh, J. R., Clinical optoacoustic imaging combined with ultrasound for coregistered functional and anatomical mapping of breast tumors. *Photoacoustics* **2018,** *12*, 30-45.
30. Zalev, J.; Richards, L. M.; Clingman, B. A.; Harris, J.; Cantu, E.; Menezes, G. L. G.; Avila, C.; Bertrand, A.; Saenz, X.; Miller, S.; Oraevsky, A. A.; Kolios, M. C., Opto-acoustic imaging of relative blood oxygen saturation and total hemoglobin for breast cancer diagnosis. *J Biomed Opt* **2019,** *24* (12), 1-16.
31. Asao, Y.; Hashizume, Y.; Suita, T.; Nagae, K. I.; Fukutani, K.; Sudo, Y.; Matsushita, T.; Kobayashi, S.; Tokiwa, M.; Yamaga, I.; Fakhrejahani, E.; Torii, M.; Kawashima, M.; Takada, M.; Kanao, S.; Kataoka, M.; Shiina, T.; Toi, M., Photoacoustic mammography capable of simultaneously acquiring photoacoustic and ultrasound images. *J Biomed Opt* **2016,** *21* (11), 116009.
32. Lin, L.; Hu, P.; Shi, J.; Appleton, C. M.; Maslov, K.; Li, L.; Zhang, R.; Wang, L. V., Single-breath-hold photoacoustic computed tomography of the breast. *Nat Commun* **2018,** *9* (1), 2352.
33. Li, J.; Chekkoury, A.; Prakash, J.; Glasl, S.; Vetschera, P.; Koberstein-Schwarz, B.; Olefir, I.; Gujrati, V.; Omar, M.; Ntziachristos, V., Spatial heterogeneity of oxygenation and haemodynamics in breast cancer resolved in vivo by conical multispectral optoacoustic mesoscopy. *Light Sci Appl* **2020,** *9*, 57.
34. Omar, M.; Schwarz, M.; Soliman, D.; Symvoulidis, P.; Ntziachristos, V., Pushing the optical imaging limits of cancer with multi-frequency-band raster-scan optoacoustic mesoscopy (RSOM). *Neoplasia* **2015,** *17* (2), 208-14.
35. Hindelang, B.; Aguirre, J.; Schwarz, M.; Berezhnoi, A.; Eyerich, K.; Ntziachristos, V.; Biedermann, T.; Darsow, U., Non-invasive imaging in dermatology and the unique potential of raster-scan optoacoustic mesoscopy. *J Eur Acad Dermatol Venereol* **2019,** *33* (6), 1051-1061.
36. Aguirre, J.; Schwarz, M.; Soliman, D.; Buehler, A.; Omar, M.; Ntziachristos, V., Broadband mesoscopic optoacoustic tomography reveals skin layers. *Opt Lett* **2014,** *39* (21), 6297-300.
37. Haedicke, K.; Agemy, L.; Omar, M.; Berezhnoi, A.; Roberts, S.; Longo-Machado, C.; Skubal, M.; Nagar, K.; Hsu, H. T.; Kim, K.; Reiner, T.; Coleman, J.; Ntziachristos, V.; Scherz, A.; Grimm, J., High-resolution optoacoustic imaging of tissue responses to vascular-targeted therapies. *Nat Biomed Eng* **2020,** *4* (3), 286-297.

38. Beziere, N.; Ntziachristos, V., Optoacoustic imaging: an emerging modality for the gastrointestinal tract. *Gastroenterology* **2011,** *141* (6), 1979-85.
39. He, H.; Buehler, A.; Bozhko, D.; Jian, X.; Cui, Y.; Ntziachristos, V., Importance of ultrawide bandwidth for optoacoustic esophagus imaging. *IEEE Transactions on Medical Imaging* **2017**, 1-1.
40. Kim, M.; Lee, K. W.; Kim, K.; Gulenko, O.; Lee, C.; Keum, B.; Chun, H. J.; Choi, H. S.; Kim, C. U.; Yang, J. M., Intra-instrument channel workable, optical-resolution photoacoustic and ultrasonic mini-probe system for gastrointestinal endoscopy. *Photoacoustics* **2022,** *26*, 100346.
41. Yang, J. M.; Favazza, C.; Chen, R.; Yao, J.; Cai, X.; Maslov, K.; Zhou, Q.; Shung, K. K.; Wang, L. V., Simultaneous functional photoacoustic and ultrasonic endoscopy of internal organs in vivo. *Nat Med* **2012,** *18* (8), 1297-1302.
42. Yang, J. M.; Maslov, K.; Yang, H. C.; Zhou, Q.; Shung, K. K.; Wang, L. V., Photoacoustic endoscopy. *Opt Lett* **2009,** *34* (10), 1591-3.
43. He, H.; Buehler, A.; Ntziachristos, V., Optoacoustic endoscopy with curved scanning. *Opt Lett* **2015,** *40* (20), 4667-70.
44. Yang, J. M.; Chen, R.; Favazza, C.; Yao, J.; Li, C.; Hu, Z.; Zhou, Q.; Shung, K. K.; Wang, L. V., A 2.5-mm diameter probe for photoacoustic and ultrasonic endoscopy. *Optics express* **2012,** *20* (21), 23944-53.
45. Viator, J. A.; Paltauf, G.; Jacques, S. L.; Prahl, S. A., Design and testing of an endoscopic photoacoustic probe for determination of treatment depth after photodynamic therapy. *Biomedical Optoacoustics II* **2001,** *4256*, 16-27.
46. Sethuraman, S.; Aglyamov, S. R.; Amirian, J. H.; Smalling, R. W.; Emelianov, S. Y., Intravascular photoacoustic imaging using an IVUS imaging catheter. *IEEE Trans Ultrason Ferroelectr Freq Control* **2007,** *54* (5), 978-86.
47. Wang, B.; Emelianov, S., Thermal intravascular photoacoustic imaging. *Biomed Opt Express* **2011,** *2* (11), 3072-8.
48. Li, X.; Wei, W.; Zhou, Q.; Shung, K. K.; Chen, Z., Intravascular photoacoustic imaging at 35 and 80 MHz. *J Biomed Opt* **2012,** *17* (10), 106005.
49. He, H.; Wissmeyer, G.; Ovsepian, S. V.; Buehler, A.; Ntziachristos, V., Hybrid optical and acoustic resolution optoacoustic endoscopy. *Opt Lett* **2016,** *41* (12), 2708-10.
50. Li, Y.; Lin, R.; Liu, C.; Chen, J.; Liu, H.; Zheng, R.; Gong, X.; Song, L., In vivo photoacoustic/ultrasonic dual-modality endoscopy with a miniaturized full field-of-view catheter. *J Biophotonics* **2018,** *11* (10), e201800034.
51. Xie, Z.; Shu, C.; Yang, D.; Chen, H.; Chen, C.; Dai, G.; Lam, K. H.; Zhang, J.; Wang, X.; Sheng, Z.; Gao, D.; Liu, C.; Song, L.; Gong, X., In vivo intravascular photoacoustic imaging at a high speed of 100 frames per second. *Biomed Opt Express* **2020,** *11* (11), 6721-6731.
52. Ansari, R.; Zhang, E. Z.; Desjardins, A. E.; Beard, P. C., Miniature all-optical flexible forward-viewing photoacoustic endoscopy probe for surgical guidance. *Opt Lett* **2020,** *45* (22), 6238-6241.
53. He, H.; Stylogiannis, A.; Afshari, P.; Wiedemann, T.; Steiger, K.; Buehler, A.; Zakian, C.; Ntziachristos, V., Capsule optoacoustic endoscopy for esophageal imaging. *J Biophotonics* **2019,** *12* (10), e201800439.
54. Ali, Z.; Zakian, C.; Li, Q.; Gloriod, J.; Crozat, S.; Bouvet, F.; Pierre, G.; Sarantos, V.; Di Pietro, M.; Flisikowski, K.; Andersen, P.; Drexler, W.; Ntziachristos, V., 360° optoacoustic capsule endoscopy at 50 Hz for esophageal imaging. *Photoacoustics* **2022,** *25*, 100333.
55. Jansen, K.; van der Steen, A. F.; van Beusekom, H. M.; Oosterhuis, J. W.; van Soest, G., Intravascular photoacoustic imaging of human coronary atherosclerosis. *Opt Lett* **2011,** *36* (5), 597-9.
56. Li, C.; Yang, J. M.; Chen, R.; Yeh, C. H.; Zhu, L.; Maslov, K.; Zhou, Q.; Shung, K. K.; Wang, L. V., Urogenital photoacoustic endoscope. *Opt Lett* **2014,** *39* (6), 1473-1476.

57. Ansari, R.; Zhang, E. Z.; Desjardins, A. E.; Beard, P. C., All-optical forward-viewing photoacoustic probe for high-resolution 3D endoscopy. *Light Sci Appl* **2018,** *7* (1), 75.
58. Zhang, E.; Laufer, J.; Beard, P., Backward-mode multiwavelength photoacoustic scanner using a planar Fabry-Perot polymer film ultrasound sensor for high-resolution three-dimensional imaging of biological tissues. *Appl Opt* **2008,** *47* (4), 561-77.
59. Zhao, T.; Pham, T. T.; Baker, C.; Ma, M. T.; Ourselin, S.; Vercauteren, T.; Zhang, E.; Beard, P. C.; Xia, W., Ultrathin, high-speed, all-optical photoacoustic endomicroscopy probe for guiding minimally invasive surgery. *Biomedical optics express* **2022,** *13* (8), 4414-4428.
60. He, H.; Buehler, A.; Bozhko, D.; Jian, X.; Cui, Y.; Ntziachristos, V., Importance of Ultrawide Bandwidth for Optoacoustic Esophagus Imaging. *IEEE Trans Med Imaging* **2018,** *37* (5), 1162-1167.
61. Liu, N.; Yang, S.; Xing, D., Photoacoustic and hyperspectral dual-modality endoscope. *Opt Lett* **2018,** *43* (1), 138-141.
62. Taruttis, A.; van Dam, G. M.; Ntziachristos, V., Mesoscopic and macroscopic optoacoustic imaging of cancer. *Cancer research* **2015,** *75* (8), 1548-59.
63. Ntziachristos, V.; Pleitez, M. A.; Aime, S.; Brindle, K. M., Emerging Technologies to Image Tissue Metabolism. *Cell Metab* **2019,** *29* (3), 518-538.
64. L.Tres, A. L. K. a. L., *Histology and Cell Biology: An Introduction to Pathology*. 3 ed.; Elsevier / Mosby; : 2011.
65. Ali, Z.; Zakian, C.; Ntziachristos, V., Ultra-broadband axicon transducer for optoacoustic endoscopy. *Sci Rep* **2021,** *11* (1), 1654.
66. Ulgen, O.; Shnaiderman, R.; Zakian, C.; Ntziachristos, V., Interferometric optical fiber sensor for optoacoustic endomicroscopy. *J Biophotonics* **2021,** *14* (7), e202000501.
67. Shnaiderman, R.; Wissmeyer, G.; Ulgen, O.; Mustafa, Q.; Chmyrov, A.; Ntziachristos, V., A submicrometre silicon-on-insulator resonator for ultrasound detection. *Nature* **2020,** *585* (7825), 372-378.
68. Wissmeyer, G.; Pleitez, M. A.; Rosenthal, A.; Ntziachristos, V., Looking at sound: optoacoustics with all-optical ultrasound detection. *Light Sci Appl* **2018,** *7*, 53.
69. Stylogiannis, A.; Prade, L.; Buehler, A.; Aguirre, J.; Sergiadis, G.; Ntziachristos, V., Continuous wave laser diodes enable fast optoacoustic imaging. *Photoacoustics* **2018,** *9*, 31-38.
70. Stylogiannis, A.; Kousias, N.; Kontses, A.; Ntziachristos, L.; Ntziachristos, V., A Low-Cost Optoacoustic Sensor for Environmental Monitoring. *Sensors (Basel)* **2021,** *21* (4).
71. Erfanzadeh, M.; Zhu, Q., Photoacoustic imaging with low-cost sources; A review. *Photoacoustics* **2019,** *14*, 1-11.
72. Stylogiannis, A.; Prade, L.; Glasl, S.; Mustafa, Q.; Zakian, C.; Ntziachristos, V., Frequency wavelength multiplexed optoacoustic tomography. *Nat Com* **2022,** *13* (1).